Performance Analysis and Optimization of DCT-Based Multicarrier System on Frequency-Selective Fading Channels

Chang He, Lei Zhang, Juquan Mao, Aijun Cao, Pei Xiao and Muhammad Ali Imran

***Abstract*—Regarded as one of the most promising transmission techniques for future wireless communications, the discrete cosine transform (DCT) based multicarrier modulation (MCM) system employs cosine basis as orthogonal functions for real-modulated symbols multiplexing, by which the minimum orthogonal frequency spacing can be reduced by half compared to discrete Fourier transform (DFT) based one. With a time-reversed prefilter employed at the front of the receiver, interference-free one-tap equalization is achievable for the DCT-based systems. However, due to the correlated pre-filtering operation in time domain, the signal-to-noise ratio (SNR) is enhanced as a result at the output. This leads to reformulated detection criterion to compensate for such filtering effect, rendering minimum-mean-square-error (MMSE) and maximum likelihood (ML) detections applicable to the DCT-based multicarrier system. In this paper, following on the pre-filtering based DCT-MCM model that build in the literature work, we extend the overall system by considering both transceiver perfections and imperfections, where frequency offset, time offset and insufficient guard sequence are included. In the presence of those imperfection errors, the DCT-MCM systems are analysed in terms of desired signal power, inter-carrier interference (ICI) and inter-symbol interference (ISI). Thereafter, new detection algorithms based on zero forcing (ZF) iterative results are proposed to mitigate the imperfection effect. Numerical results show that the theoretical analysis match the simulation results, and the proposed iterative detection algorithms are able to improve the overall system performance significantly.**

***Index Terms*—Discrete cosine transform (DCT), fading channels, intercarrier interference (ICI), performance optimization.**

I. Introduction

In addition to some famous waveforms such as orthogonal frequency division multiplexing (OFDM) [1], universal filtered multi-carrier (UFMC) [2], [3], [4], generalized frequency division multiplexing (GFDM) [5], filter bank multi-carrier (FBMC) [6], [7], filtered OFDM [4], [8], the discrete cosine transform (DCT) based multicarrier modulation (MCM) is one of the spectrally-efficient transmission candidates for the next generation wireless communications. Under the restriction that only real-valued signals are transmitted, it supports the minimum subcarrier spacing at $1/(2T)$ Hz instead of $1/T$ in OFDM by adopting cosinusoidal orthogonal functions $\cos(2\pi \times kt/(2T))$ [9], where T is the symbol period and k is the subcarrier index respectively. Correspondingly, the multiplexing and de-multiplexing operations for all information carried subcarriers can be simply performed by discrete cosine transform (DCT) pair, which is similar to what discrete Fourier transform (DFT) pair did in OFDM systems. However, the fast DCT algorithms proposed in [10] and [11] provide some improvements in computation complexity when compared with fast Fourier transform (FFT) algorithms. But the complexity reduction is limited, compared with the order of N^2 in general for a length-N sequence [12]. Additionally, similar to other real-transform techniques for multicarrier systems (e.g. DHT-based MCM [13], [14], [15]), the DCT uses only real arithmetic along with real-valued signals. As a result, the employed system does not need a quadrature modulator at the transmitter, thus avoiding the in-phase/quadrature-phase (I/Q) imbalance problem. In addition to avoiding IQ imbalance, it also reduces phase noise sensitivity. This can further reduce both the signal-processing complexity and power consumption at the transmitter implementation [10], which is very attractive for massive machine-type communications (mMTC) where transmitter devices for power efficiency and low complexity are always desired to support more user equipments [16]. The study in [12] shows analytically that in the presence of frequency offset, inter-carrier interference (ICI) coefficients are more concentrated around the central coefficients in DCT-MCM than in DFT-MCM, bringing enhanced robustness against frequency offsets. This renders DCT-MCM very promising for some high-speed mobility communication scenarios such as railway dedicated mobile communication systems where high Doppler shifts have a major impact on the overall system performance [17].

Despite of those merits, one major designing difficulty that DCT-MCM schemes encounter in practical design is that when the system is employed under multipath fading channels, the circular convolution property by DCT does not hold and, therefore the cyclic-prefix (CP) based approaches used in conventional OFDM systems do not apply any more [18], [19]. The convolution property by DCT has been demonstrated in seminal work in [20], which implies the fact that the equivalent channel matrix can only be diagonalized by DCT when the channel impulse response (CIR) is symmetric. The chromatic dispersion channel in single-mode fibres (SMFs) [21] is one of the examples which meets the specified symmetry condition,

The material in this paper was presented in part at the 2016 IEEE International Symposium on Wireless Communication Systems.

C. He, J. Mao and P. Xiao are with the Institute for Communication Systems (ICS), University of Surrey, Guildford, GU2 7XH, UK. (Email:{c.he, juquan.mao, p.xiao}@surrey.ac.uk.)

L. Zhang and M.A Imran are with School of Engineering, University of Glasgow, Glasgow, G12 8QQ, Scotland (Email:{Lei.Zhang, Muhammad.Imran}@glasgow.ac.uk)

Aijun Cao is with ZTE R&D center in Stockholm, Sweden, 164 51 Kista (Email:cao.aijun@zte.com.cn).

but it only works in optical communications. In the case of generic circumstances, such as wireless multipath fading channels, the transmitting signals and CIR in time domain is not symmetrically convoluted, and the channel cannot be compensated by simple one-tap equalizers exploiting CP accordingly.

In the literature, various attempts exist trying to sidestep this problem. The earlier proposed method in [22] extends the post-DCT signal symmetrically in double length to address the symmetry issue, however, losing the data rate by half as an expense. A more effective method without data rate sacrifice is based on zero-padding algorithm [12], by which guard sequence is zero inserted to eliminate ISI caused by multipath. But it destroys the orthogonality and the residual ICI limits overall system performance. Another alternative solution is called cosine modulated multitone (CMT) based FBMC, in which ICI issue is mitigated and made less crucial through a bank of well-designed filters than with other schemes [6]. However, the significantly increased complexity and some other practical system configuration problems hinders its practical deployment. Besides the above designing approaches, an optimized solution is inspired by Al-Dhahir in [18], where one-tap equalization is enabled in the cosine domain by using a time-reversed filter at the front of receiver so that CIR symmetry is acquired after filtering. Unlike conventional DFT-MCM system where CP is normally added at each transmission block, this optimised method has to introduce both prefix and suffix as symmetrically extended sequence from the information block and the information symbol should be one-dimensional formatted. With these two constraint conditions satisfied, a one-tap equalizer is applicable to achieve the optimum performance for DCT-MCM under wireless frequency-selective channels.

To the best of our knowledge, previous work described in [18] and [23] have built fundamental framework for the prefiltering based DCT-MCM systems in the form of matrix expressions. System optimizations for one-tap equalization procedure has also been investigated. In order to provide in-depth insights into the prefiltering mechanism for DCT-MCM, especially its effects on the output SNR performance, an alternative approach to system implementation is developed to process the signals in time domain. In this paper, following the fundamentals that laid out in the previous work in [24], we complement the theoretical basis for the employment of DCT-MCM system over frequency-selective channels and systematically extend our study by considering both transceiver perfections and imperfections. Corresponding theoretical results are derived as well in formula. The novelties and contributions of this paper are summarized as follows:

- The output SNR expression per subcarrier is derived by taking the pre-filtering effect into account. With the provision of additional analysis on the lower boundary for the minimum received signal power, the output SNR gain is verified between among all subcarriers, compared to DFT-MCM system.
- In addition to conventional zero forcing (ZF) detection technique that has been employed in most of the DCT-MCM systems, we reformulate two improved detection methods. Both of them could effectively compensate the coloured noise effect after prefiltering at the receiver. Comparisons are conducted and their BER performance are presented as well.
- In the presence of transceiver imperfections for DCT-MCM system, we implement an analytical expression in terms of desired signal, ICI and inter-symbol interference (ISI) by considering carrier frequency offset (CFO), timing offset (TO) and insufficient guard sequence between symbols. Based on the framework, zero forcing based (ZF-based) iterative channel detection algorithms are proposed and hence provide significant gain compared with conventional detection methods in terms of BER performance.

The rest of the paper is organized as following sections. We begin with Section II by demonstrating the constraint conditions and the appropriate transmission formulations for proposed optimum DCT-MCM systems. Section III improves the system model to matrix formulations and gives analysis on the pre-filtering effect on both transmitted signal power and coloured noise variance. In Section IV, by taking the prefiltering effect into account, we present reformulated criterion for conventional detection methods. In the presence of considered imperfections, we complete the received signal expression in terms of CFO, TO and insufficient guard sequence and propose corresponding effective detection algorithm to combat interference in Section V. Lastly, we draw our conclusions in Section VI.

Notations: operator $*$ is denoted as a linear convolution of two vectors. $\mathbf{I}_N$ and $\mathbf{J}_N$ stand for identity matrix and reversal matrix in dimension $N \times N$, respectively. And $\mathbf{0}_{M\times N}$ is the zero matrix of size $M \times N$. $E[\cdot]$ means taking the expectation of random variable. $[\cdot]^H$ and $[\cdot]^T$ refer to hermitian conjugate and transpose operation, respectively. $diag(\cdot)$ is defined to return the vector of the main diagonal elements of the operated matrix.

II. CONSTRAINT CONDITIONS ON DCT-MCM SYSTEM

In this section, we start by introducing the basic constraint conditions for DCT-MCM based systems and its appropriate formation to support data transmission.

In conventional DFT-MCM systems like OFDM, the absolute orthogonality that maintained among subcarriers is achieved by the complex exponential function sets and the minimum subcarrier frequency spacing ΔF is $1/T$ accordingly. However, by transmitting only one-dimensional symbols and employing a single set of cosinusoidal functions as orthogonal sets, this minimum subcarrier frequency spacing can be reduced to $\Delta F = 1/2T$ in the sense that:

$$\int_0^T \sqrt{\frac{2}{T}}\cos\left(2\pi k\Delta F t\right)\sqrt{\frac{2}{T}}\cos\left(2\pi m\Delta F t\right)dt = \begin{cases} 1, k = m \\ 0, k \neq m \end{cases} \tag{1}$$

Particularly, in DCT-MCM systems, modulator and demodulator can be easily realized with the IDCT and DCT operation, respectively. In order to implement a simple equalizer structure by means of a bank of scalars at the receiver, the symmetric convolution-multiplication property of the DCT is exploited

to perform an element-by-element multiplication in the corresponding discrete trigonometric domain. Therefore, the guard sequence is to be duplicated as prefix and suffix. An additional time-reversed prefilter is introduced to enforce the equivalent channel impulse response to be symmetric as required. For instance, assuming a complex equivalent channel impulse after prefiltering denoted by $h(t) = h_R(t) + jh_I(t)$, then the real and imaginary components of it both satisfy the symmetric CIR constraint: $h_R(t) = h_R(-t)$ and $h_I(t) = h_I(-t)$.

In general, there exist eight types of DCT [25]. By exploiting their corresponding type of symmetry in the symbol sequence, the constraint on channel conditions and suitable symbol structure formations to use any type of DCT are presented for data transmission in [26]. Their corresponding channel estimation techniques, based on the use of training symbols, also taking into account their special symmetric conditions in the time domain for any kind of DCT, are presented in [23]. Since the results indicate that every kind of DCT achieves identical performance [23], [26] without loss of generality, here we only consider the type-II DCT pair for multiplexing and demultiplexing for simplicity as it earns great popularity in most of the practical DCT-based transceiver implementations [25]. The baseband modulated discrete-time signal x_m in a N subcarrier DCT-MCM system is then represented by

$$x_m = \sum_{k=0}^{N-1} a_k \beta_k \cos[\frac{\pi k(2m+1)}{2N}], \quad m = 0, 1, \cdots, N-1. \tag{2}$$

where a_k is amplitude-shift keying (ASK) modulated information symbol that transmitted on the kth subcarrier and the parameter coefficient β_k is defined as

$$\beta_k = \begin{cases} \sqrt{\frac{1}{N}}, & k = 0 \\ \sqrt{\frac{2}{N}}, & k = 1, 2, \cdots, N-1 \end{cases} \tag{3}$$

To completely avoid the ICI and ISI problems, the length of the prefix and suffix v should be at least equal to the channel delay spread. [18] has given the symmetric extension for the prefix and suffix as follows:

$$\begin{aligned} x_{-n} &= x_{n-1}, \quad 1 \le n \le v \\ x_{N-1+n} &= x_{N-n}, \quad 1 \le n \le v \end{aligned} \tag{4}$$

Assuming the real component vector of CIR with L taps is $\mathbf{f}_r = [f_0, f_1, \ldots, f_{L-1}]$. Its corresponding time-reversed filter vector is thus in the reverse form $\mathbf{g}_r = [f_{L-1}, f_{L-2}, \ldots, f_0]$, resulting in the overall effective symmetric channel vector:

$$\begin{aligned} \mathbf{h}_r &= \mathbf{f}_r * \mathbf{g}_r = [f_0, f_1, \ldots, f_{L-1}] * [f_{L-1}, \ldots, f_1, f_0] \\ &= [h_{-L+1}, h_{-L+2}, \ldots, h_0, \ldots, h_{L-2}, h_{L-1}] \end{aligned} \tag{5}$$

where $\mathbf{h}_r = [h_{-L+1}, h_{-L+2}, \ldots, h_0, \ldots, h_{L-2}, h_{L-1}]$ is denoted as the effective CIR vector for real branch with delay spread at length $2L-1$. By which the element h_n in the vector is represented as a convolution result as

$$h_n = \begin{cases} \sum_{k=0}^{L-|n|} f_k f_{k+|n|} & \text{if } -L+1 \le n \le L-1; \\ 0 & \text{others.} \end{cases} \tag{6}$$

Apparently, the symmetry property arises with the condition $h_n = h_{-n}$ implied in the aforementioned. The effective channel response coefficients corresponding to those one-tap per subcarrier equalizers is obtained in [26]:

$$H_k = 2\sum_{n=1}^{L-1} h_n \cos[\frac{\pi k n}{N}] + h_0, \quad k = 0, 1, \cdots, N-1. \tag{7}$$

With the above condition constraints provided, we are now able to formulate the pre-filtering method model and present further system analysis for the DCT-MCM system in multipath fading environments.

III. System model and Output SNR Analysis

Due to the correlated pre-filtering in time domain, the signal power is no longer equally spread among subcarriers. For the purpose of analysing the pre-filtering effect on DCT-MCM systems over general multipath fading channels, the baseband equivalent system model is proposed in the form of matrix representation. Mathematical representations for ergodic output signal power and coloured noise variance are then provided, respectively.

Note that in DCT-MCM systems, the symbols that are ready for transmission are all in real format after multiplexing by IDCT. Consequently, the convolution with a complex-valued CIR can be regarded as two independent processes that the signal is convolved with the real component and imaginary component of the CIR at the same time, with each allocating one-half of the total signal power. As to the pre-filtering, the received signals after channel are firstly separated by quadrature. Then both the real and imaginary components of received signals are fed to their corresponding prefilter vectors respectively as indicated in Fig. 1 [24]. Due to the orthogonality maintained between in-phase and quadrature branches, the detector is able to recover the information bits from either real part or imaginary part of received signals. To make full use of the information, the two independently filtered data streams are combined in complex form for detection. Since the two streams experience identical signal processing steps in quadrature, without loss of generality, the following derivations are for in-phase branch and we focus on real signals processing mechanism. The total output signal power thus can be obtained by doubling.

A. system model

Assuming N ASK modulated symbols are allocated to N subcarriers at the transmitter. The general transmission system model on in-phase branch in the diagram is expressed as [23], [24]

$$\mathbf{y} = \mathbf{DRP}_R\mathbf{H}_R\mathbf{CD}^H\mathbf{a} + \mathbf{DRP}_R\mathbf{n}_R \tag{8}$$

where $\mathbf{y}$ is the demodulated signal vector to be equalized, $\mathbf{a} \in \mathbb{R}^{N\times 1}$ is information symbol vector with normalized signal power ($\sigma_s^2 = 1$). $\mathbf{D} \in \mathbb{R}^{N\times N}$ is type-II DCT matrix that has been power normalized and its (l, m) entry is given by

$$d_{l,m} = \begin{cases} \sqrt{\frac{2}{N}} \cos(\frac{(l-1)(2m-1)\pi}{2N}), & l > 1 \\ \sqrt{\frac{1}{N}}, & l = 1. \end{cases} \tag{9}$$

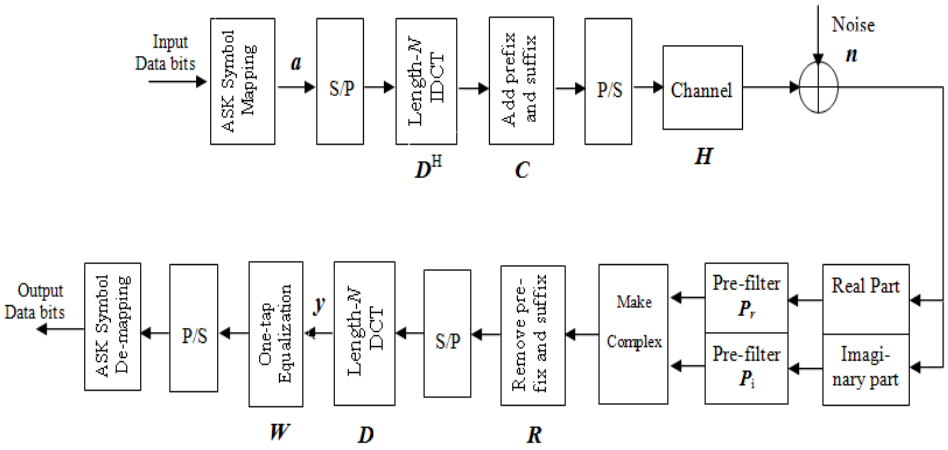

Fig. 1. Baseband system model for pre-filtering DCT-MCM systems

$\mathbf{C} \in \mathbb{R}^{(N+2v)\times N}$ is a prefix and suffix inserting matrix at length v which is organized as $\mathbf{C} = [\mathbf{J}_v, \mathbf{0}_{v\times(N-v)}; \mathbf{I}_N; \mathbf{0}_{v\times(N-v)}, \mathbf{J}_v]$. Generally, we assume the prefix and suffix have the same guard sequence length and the whole block length is $L_1 = N + 2v$. The multi-path channel convolution matrix on in-phase branch $\mathbf{H}_R \in \mathbb{R}^{L_1\times L_1}$ is implemented as a Toeplitz matrix with the first row and first column being $[f_{L-1}, f_{L-2}, \ldots, f_0, \mathbf{0}_{1\times(L_1-L)}]$ and $[f_{L-1}, \mathbf{0}_{1\times(L_1-1)}]^T$ respectively. In order to achieve free ISI transmission, sufficient guard sequence length should be met by $L \leq v$ [18]. The pre-filter matrix $\mathbf{P}_R \in \mathbb{R}^{L_1\times L_1}$, which stands for time-reverse filtering on in-phase branch, is also implemented by a Toeplitz matrix with its first row and column being $[f_{L-1}, \mathbf{0}_{1\times(L_1-1)}]$ and $[f_{L-1}, f_{L-2}, \ldots, f_0, \mathbf{0}_{1\times(L_1-L)}]^T$, respectively. The guard sequence discarding operation is defined by $\mathbf{R} \in \mathbb{R}^{N\times L_1}$ and we build it in the form as

$$\mathbf{R} = [\mathbf{0}_{N\times v}, \mathbf{I}_N, \mathbf{0}_{N\times v}]. \tag{10}$$

According to the aforementioned constraint conditions, with the employment of a pre-filter and insertion of symmetric guard sequence, the DCT-MCM is optimised for information carrying without ICI and ISI problems. This renders the output of $\mathbf{DRP}_R\mathbf{H}_R\mathbf{CD}^H$ integration equivalent to a diagonal matrix by which the relation is given by

$$\mathbf{H}_{eff,R} = \mathbf{DRP}_R\mathbf{H}_R\mathbf{CD}^H \tag{11}$$

where $\mathbf{H}_{eff,R} \in \mathbb{R}^{L_1\times L_1}$ is the effective channel matrix for in-phase branch and the elements on the diagonal vector is defined as

$$diag(\mathbf{H}_{eff,R}) = [H_0, H_1, \ldots, H_{N-1}] \tag{12}$$

where H_k is the effective frequency response coefficient that has been provided in Eq. (7).

In conventional DFT-MCM systems, it is assumed that the channel frequency responses subject to Gaussian distribution with equal power for all subcarriers if a typical Rayleigh fading channel is considered. However, due to the correlated pre-filtering, the output signal power is not identically distributed among subcarriers in DCT-MCM systems. In order to get an in-depth look at the output SNR, we present our analysis on output signal power and noise variance as below, respectively.

B. Ergodic Output Signal Power

In practice, many wireless multipath fading channels are modelled as Rayleigh fading channels having an impulse response represented by a tapped delay line where coefficients are Gaussian random process [27]. As a consequence, here we denote the in-phase component of channel coefficients as $f_k \sim N(0, 0.5\sigma_k^2)$. Considering the channel is already normalised with power, we get

$$\sum_{k=0}^{L-1} \sigma_k^2 = 1 \tag{13}$$

Upon the assumption that channel taps are independent to each other, we have

$$E[f_i \cdot f_j] = 0 \quad \text{if } i \neq j \tag{14}$$

By combining Eq. (6) and Eq. (14), the expected correlation results for effective channel coefficients is obtained as (see Appendix A)

$$E[h_i \cdot h_j] = \begin{cases} \frac{1}{4}\sum_{p=0}^{|i|} \sigma_p^2\sigma_{L-|i|+p}^2 & i = \pm j \neq 0; \\ \frac{3}{4}\sum_{p=0}^{L-1} \sigma_p^4 + \frac{1}{2}\sum_{p=0}^{L-1}\sum_{t=0}^{L-1-p} \sigma_p^2\sigma_{p+t}^2 & i = j = 0; \\ 0 & \text{others.} \end{cases} \tag{15}$$

By substituting Eq. (15) to Eq. (7), the ergodic output signal power on in-phase branch at kth subcarrier is

$$E[H_k^2] = E[h_0^2] + 4\sum_{n=1}^{L-1} E[h_n^2] \cdot \cos^2[\frac{\pi}{N}nk] \tag{16}$$

From Eq. (16), it is obvious to see that the subcarriers are subject to diverse gain and we are able to define the boundaries for the gain variation.

As depicted apparently in the signal gain equation, the signal power will be maximized if the multiplying term

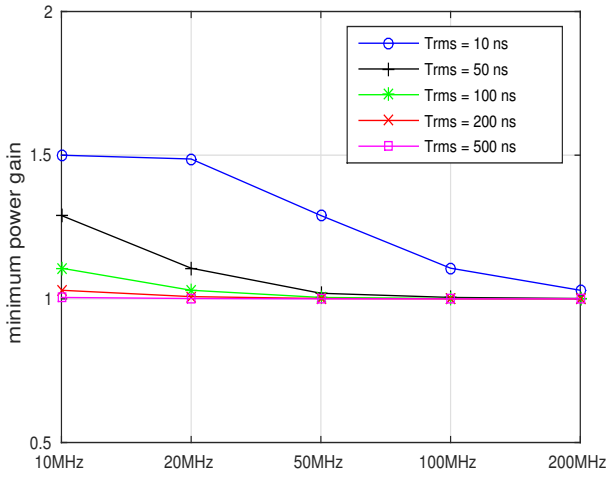

Fig. 2. The minimum signal power gain for different sampling frequency and RMS delay in a typical IEEE 802.11 channel.

$\cos^2[\frac{\pi}{N}nk]$ achieves the maximum value at 1, which is always obtained by the initial subcarrier at index $k = 0$, i.e.,

$$\begin{aligned} E[H_0^2] &= E[h_0^2] + 4\sum_{n=1}^{L-1} E[h_n^2] \\ &= \frac{3}{4}\sum_{p=0}^{L-1}\sigma_p^4 + \frac{3}{2}\sum_{p=0}^{L-1}\sum_{t=0}^{L-1-p}\sigma_p^2\sigma_{p+t}^2 = 0.75 \end{aligned} \tag{17}$$

This indicates that, for a power normalised channel case, $E[H_0^2]$ is irrelevant to channel characteristics and equals to a constant value at 0.75. Accounting for the other half of distributed signal power on quadrature branch which experience similar signal processing, the total output signal power on the initial subcarrier is reached to the upper bound at gain of 1.5.

The power gain for other subcarriers are below the upper boundary, i.e., $E[H_k^2] \leq E[H_0^2]$. The minimum gain, on the other hand, is variable and subject to the channel type and its channel parameters. However, In Appendix B, we have proved the lower bound for the minimum gain is $1 + \frac{1}{2L}$ when the channel has L taps. Our simulation results are in agreement with this analysis as indicated in Fig. 2 where we give an example of typical IEEE 802.11 channels [28] with different sampling frequency and root mean square (RMS) delay spread. When the RMS is 10ns and sampling frequency is 10MHz, which is a single-tap case, the minimum power gain is thus 1.5. As the channel tap increases (either by increasing the sampling frequency or the RMS delay spread), this minimum gain will gradually reduce and finally coincide with the lower bound at a certain point to 1, which is identical with analysis shown above.

C. Coloured Noise Variance

The pre-filtering operation also affects the coloured noise variance as well. As the pre-filtering is operated independently on in-phase and quadrature branches, after filtering, the coloured noise $\mathbf{v}$ is combined by real and imaginary components which is expressed as

$$\mathbf{v} = \mathbf{DR}(\mathbf{P}_R\mathbf{n}_R + j\mathbf{P}_I\mathbf{n}_I) \tag{18}$$

where $\mathbf{P}_R$ and $\mathbf{P}_I$ are for real and imaginary parts pre-filtering; whereas $\mathbf{n}_R$ and $\mathbf{n}_I$ are the components of the AWGN channel noise vector $\mathbf{n}$ with variance σ_n^2 in quadrature. The expectation for the coloured noise covariance matrix $E[\mathbf{v}\mathbf{v}^H]$, proven in [24], is in the form of an identical matrix multiplying a constant factor, which is represented as

$$E[\mathbf{v}\mathbf{v}^H] = 0.5\sigma_n^2 \cdot \mathbf{I}_N \qquad \text{if } L \leq v \tag{19}$$

This reveals that by independently filtering the in-phase and quadrature branches, the resulted coloured noise variance after combiner is reduced by half. The key to this variance reduction lies to the fact that modulated symbols after IDCT are in one-dimensional format for transmission, hence become robust against the complexed noise.

D. Output SNR gain

The ergodic output SNR can be represented in terms of input SNR, output signal power and coloured noise variance. The input SNR is defined as

$$SNR_{in} = \frac{\sigma_s^2}{\sigma_n^2} \qquad \text{for all subcarriers} \tag{20}$$

Accounting for the pre-filtering effect and power loss form guard sequence insertion, the output SNR at kth subcarrier is in the form as

$$\begin{aligned} SNR_{out}(k) &= \frac{N}{N+2v} \cdot \frac{2E[H_k^2] \cdot \sigma_s^2}{0.5\sigma_n^2} \\ &= \frac{4N \cdot E[H_k^2]}{N+2v} \cdot SNR_{in}(k) \end{aligned} \tag{21}$$

Since $1 \leq 2E[H_k^2] \leq 1.5$, we get a proposition for the achieved output SNR gain.

Proposition: Consider a DCT-MCM system, the pre-filtering process will achieve a output SNR gain between $\frac{2N}{N+2v}$ and $\frac{3N}{N+2v}$ for all subcarriers.

Consequently, the exact gain η of output SNR obtained for arbitrary subcarrier index is

$$\eta(k) = \frac{4N}{N+2v}(E[h_0^2] + 4\sum_{n=1}^{L-1} E[h_n^2]\cos^2[\frac{\pi}{N}nk]) \tag{22}$$

Eq. (22) implies the output SNR gain is subject to employed subcarrier number and channel characteristics. We then can take a look at the exact SNR gain at the output of the receiver. Fig. 3 demonstrates the simulation results for output SNR gain with respect to three widely employed channels, which are named by, Extended Pedestrian A model (EPA), Extended Typical Urban model (ETU) and Extended Vehicular A model (EVA), respectively. In practice, the channel knowledge is obtained through the introduction of pilot symbols and the channel state will not change within one transmitted symbol in slowly fading environments [23], [29]. Here we ignore the channel imperfection issues and assume information is perfectly known at the receiver. The sampling rate for simulation

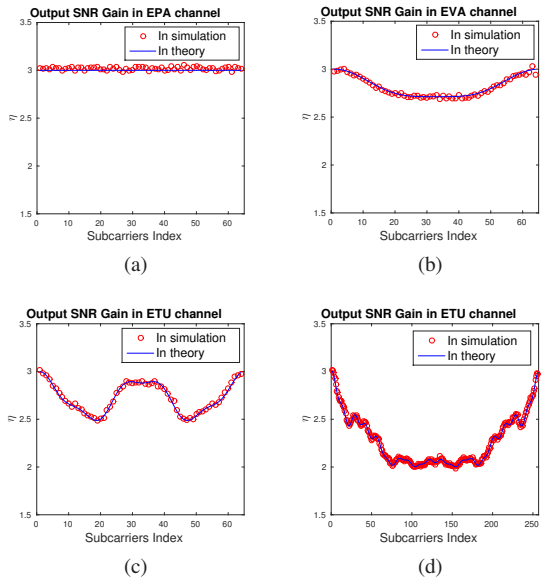

Fig. 3. The output SNR gain achieved in three typical channels. (a) EPA N=64. (b) EVA N=64. (c) ETU N=64 (d) ETU N=256. [24].

is assumed at f_s=20MHz and we assign 64 and 256 subcarriers separately to the system for comparison. Considering the SNR loss from prefix/suffix insertion is fixed and not relevant to the pre-filtering process, without loss of generality, we neglect the effect form the term $\frac{N}{N+2v}$ in the simulation.

As can be seen in Fig. 3, for all subcarriers, our simulation results on the linear gain η for all kinds of channels concur with the previous analysis in Eq. (22). The sub-figures (a),(b) and (c) give very distinct variation trends under different channel characteristics. Generally, the output SNR gain varies in the range between 2 to 3 folds among all subcarriers, which is verified in our proposition. In particular, as depicted in the figures, the gain variation curves fluctuate sharply along with increased allocated subcarrier number and channel taps. Fig 3. (a), due to the flat fading case in the sense of a EPA channel at f_s=20MHz, in particular, achieves a constant gain at $\eta = 3$ for all subcarriers. The cosine term, as indicated on the right in Eq. (22), brings the symmetry property to the gain variation curves, which is clearly observed at the middle subcarrier index on all accounts.

IV. Reformulated Criterion for DCT-MCM System Detections

In this section, three commonly used detection techniques are discussed to be integrated with DCT-MCM systems. Among of the three, the zero forcing (ZF) one-tap equalizer is easy and efficient to build at the receiver [30] without the need for noise information. However, at frequencies where channel frequency response (CFR) is severely attenuated, the noise power is proportionally increased when the equalizer attempts to boost the signal power. As another alternatives, minimum-mean-square-error (MMSE) and maximum likelihood (ML) detections could sidestep the SNR degradation problem but require the information of CIR and the noise statistic property [31]. However, as indicated in the aforementioned section, the pre-filtering process renders the coloured noise correlated among subcarriers, therefore deviates from the Gaussian distribution. This motivates us to compute the coloured noise power at each instant and reformulate the criterion for MMSE and ML methods to make them adaptable for DCT-MCM so as to bring performance enhancement.

A. Reformulated MMSE Detection

As an alternative detection method, the MMSE equalizer is considered to compress the mean square error to the minimum [30]. To facilitate derivation, the post-DCT symbol vector is represented in terms of effective channel matrix for real part $\mathbf{H}_{eff,R}$ and imaginary part $\mathbf{H}_{eff,I}$. Combining with effective pre-filtering matrix $\mathbf{G}_R$ and $\mathbf{G}_I$ imposed on the noise, the received signal vector in Eq. (14) is simplified to

$$\begin{aligned}\mathbf{y} &= (\mathbf{H}_{eff,R} + j\mathbf{H}_{eff,I})\mathbf{a} + \mathbf{G}_R\mathbf{n}_R + j\mathbf{G}_I\mathbf{n}_I \\ &= \mathbf{H}_{eff}\mathbf{a} + \mathbf{G}_R\mathbf{n}_R + j\mathbf{G}_I\mathbf{n}_I \end{aligned} \quad (23)$$

Where $\mathbf{G}_R = \mathbf{DRP}_R$ and $\mathbf{G}_I = \mathbf{DRP}_I$. And $\mathbf{H}_{eff}$ is the complex effective channel matrix. In ZF detections, as the equalizer represented in matrix form by $\mathbf{W}_{ZF} = \mathbf{H}_{eff}^H/|\mathbf{H}_{eff}|^2$ only requires estimated CIR, conventional detection criterion can be directly used for DCT-MCM systems. However, in the case of MMSE detection method, accounting for the pre-filtering effect, the filtered noise vector $\mathbf{G}_R\mathbf{n}_R + j\mathbf{G}_I\mathbf{n}_I$ in Eq. (23) becomes coloured by multiplying a correlation matrix on both the real and imaginary components. In what follows, we provide the optimum and suboptimum MMSE detections for DCT-MCM, respectively. Since the noise correlation matrices $\mathbf{G}_R$ and $\mathbf{G}_I$ are non-diagonal inherently, the optimum MMSE detection therefore is non-linear and the overall complexity grows exponentially with the matrix size. On the other hand, the suboptimum subcarrier-wise MMSE case is a linear detction and attains the same complexity order as the ZF case.

Firstly, we assume the MMSE equalizer matrix which can effectively compensate the correlation effect is formed as $\mathbf{W}^{op}$, by taking $\frac{\partial tr E|\mathbf{W}^{op}\mathbf{y}-\mathbf{a}|}{\partial \mathbf{W}^{op}} = 0$, we have

$$\mathbf{W}^{op} = \frac{\sigma_s^2\mathbf{H}_{eff}^H}{\sigma_s^2\mathbf{H}_{eff}\mathbf{H}_{eff}^H + \frac{1}{2}\sigma_n^2(\mathbf{G}_R\mathbf{G}_R^H + \mathbf{G}_I\mathbf{G}_I^H)} \quad (24)$$

In order to reduce the general detection complexity from subcarrier-wise perspective, we take the overall correlation effect from the neighbouring subcarriers as a whole factor and calculate the noise power at each instant for the desire subcarrier. Then, the received symbol on kth subcarrier from Eq. (23) can be extracted simply to:

$$y_k = H_k a_k + \sum_{t=1}^{N} g_{k,t} n_{r,t} + j\sum_{t=1}^{N} q_{k,t} n_{i,t} \quad (25)$$

where $n_{r,t}$ and $n_{i,t}$ are the in-phase and quadrature components of noise vector $\mathbf{n}$ on subcarrier index t; whereas $g_{k,t}$ and $q_{k,t}$ are the entries from the kth row and tth column of $\mathbf{G}_R$ and $\mathbf{G}_I$, respectively. It is noted that, the coefficients $g_{k,t}$ and $q_{k,t}$ in the pre-filtering matrix are time-reversed transforms from CIR. In practice, the noise changes much faster than the channel and we can assume the channel coherent time is long over symbols. Upon that assumption, $g_{k,t}^2$ and $q_{k,t}^2$ are

regarded as instant values and the coloured noise on arbitrary subcarrier index is in the additions of Gaussian noise variables with power spectrum $N_o/2$ ($\frac{N_0}{2} = \sigma_n^2$) from all subcarriers. The coloured noise variance V_k at subcarrier index k is then calculated as

$$V_k = \frac{N_0}{2}(\sum_{t=1}^{N} g_{k,t}^2 + \sum_{t=1}^{N} q_{k,t}^2) \tag{26}$$

With the provision of the instantaneous coloured noise variance V_k, we yield the reformulated expression of the suboptimum MMSE equalizer for kth subcarrier

$$W_k^{sub} = \frac{\sigma_s^2 H_k^H}{\sigma_s^2 |H_k|^2 + V_k} \tag{27}$$

As evidenced by the above equation, the pre-filtering effect is compensated by the MMSE equalizer for DCT-MCM systems, as the coloured noise power varies at different instants.

B. Maximum Likelihood Detection

The ML detection is an outstanding solution that obtains optimal performance among the three. The detector considers all potential realizations by searching for all possible signal constellation. By assuming the raw bit value can be either zero or non-zero, a log-likelihood ratio (LLR) based detector is employed to give the logarithm of the ratio of a posteriori probabilities of the modulated symbols. In our case, the conditional probability density function of y_k given a_k is in the form as $p(y_k|a_k) = \frac{1}{\sqrt{\pi V_k}} \exp(-\frac{|y_k - H_k a_k|^2}{V_k})$. This holds for a specific information data frame for which the V_k stands for instantaneous coloured noise variance. In general, soft information in the form of the LLR indicates the confidence of demapping decision. In this regard, according to [32], the soft information contained at the ith bit is represented as

$$\begin{aligned} L_i &= \ln \frac{\sum_{a_k \in \mathcal{A}_i^{(1)}} p(a_k|y_k)}{\sum_{a_k \in \mathcal{A}_i^{(0)}} p(a_k|y_k)} = \ln \frac{\sum_{a_k \in \mathcal{A}_i^{(1)}} p(y_k|a_k)}{\sum_{a_k \in \mathcal{A}_i^{(0)}} p(y_k|a_k)} \\ &= \ln \frac{\sum_{a_k \in \mathcal{A}_i^{(1)}} \exp(\frac{-|y_k - H_k a_k|^2}{V_k})}{\sum_{a_k \in \mathcal{A}_i^{(0)}} \exp(\frac{-|y_k - H_k a_k|^2}{V_k})} \end{aligned} \tag{28}$$

where $\mathcal{A}_i^{(\lambda)}$ is the set of all possible candidate ASK symbols corresponding to $b_i = \lambda, \lambda \in \{0, 1\}$. With the provision of log-sum-exponential approximation property: $\log \sum_i \exp(\phi_i) = \max_i(\phi_i)$, after taking out the CFR effect and assuming the ZF equalized symbol on the kth subcarrier is $z_k = y_k/H_k$, and the LLR equation is simplified to

$$\begin{aligned} L_i &\approx \ln \frac{\max_{a_k \in \mathcal{A}_i^{(1)}} \exp[-|H_k|^2 (z_k - a_k)^2 / V_k]}{\max_{a_k \in \mathcal{A}_i^{(0)}} \exp[-|H_k|^2 (z_k - a_k)^2 / V_k]} \\ &= \frac{V_k}{|H_k|^2} \{ \max_{a_k \in \mathcal{A}_i^{(1)}} [-(z_k - a_k)^2] - \max_{a_k \in \mathcal{A}_i^{(0)}} [-(z_k - a_k)^2] \} \\ &= \frac{V_k}{|H_k|^2} \{ - \min_{a_k \in \mathcal{A}_i^{(1)}} (z_k - a_k)^2 + \min_{a_k \in \mathcal{A}_i^{(0)}} (z_k - a_k)^2 \} \end{aligned} \tag{29}$$

As indicated, the pre-filtering effect on both signal and noise components are compensated on the part $\frac{V_k}{|H_k|^2}$ in Eq. (34), leading to optimum system performance for DCT-MCM systems.

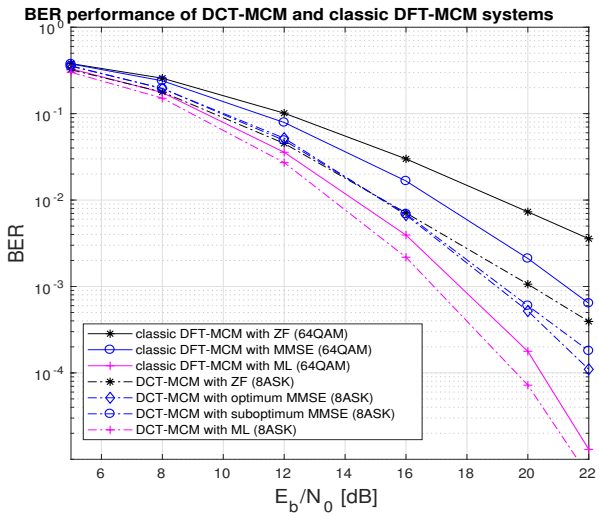

Fig. 4. BER performance for DCT-MCM and DFT-MCM systems in three detection methods

C. Performance Comparison with DFT-MCM systems

The BER performance of DCT-MCM systems is plotted in Fig. 4 with respect to the above three reformulated detection methods under a typical IEEE 802.11 channel. As indicated in [12] that the bandwidth of a DCT-MCM system by transmitting one-dimensional formatted signals can be only half of that required by a classic DFT-MCM system with the same number of subcarriers, in order to make a fair comparison with DFT-MCM systems in the sense of same bandwidth efficiency, we assign 128 number of 8ASK modulated subcarriers to DCT-MCM and 64 number of 64 quadrature amplitude modulation (64QAM) subcarriers to DFT-MCM systems respectively. A CP length of 12 is guaranteed for DFT-MCM whereas it is doubled in DCT-MCM. Additionally. the channel is coded with the polynomial (133,171) code at constraint length of 7 and rate of 1/2 for both systems. As shown in Fig. 4, due to the output SNR gain that explained in proposition 4, DCT-MCM systems outperform DFT-MCM based ones on all situations. It can also be observed that our proposed suboptimum MMSE equalizer can approach the performance of the optimum MMSE while reducing the detection complexity significantly. On the other hand, since typically the detection of less dense symbols is more robust to noise, DCT-MCM systems can result in improved error-rate performance when operating far from the capacity limit. This is verified by the superiority gap of ZF at 4dB at a BER of 10^{-2} and MMSE at 2dB at a BER of 10^{-3} between these two systems. . However, it is reduced to around 1dB at a BER of 10^{-4} if the optimum ML approach is used for the two systems, which is seen in the figure.

V. Imperfection Analysis and Equalization Algorithm

In the previous section, we focus on the performance analysis on the DCT-MCM system with perfect transceiver and sufficient guard sequence. However, in practice, due to the hardware impairments and inaccurate synchronization errors,

a certain level of CFO and TO will always be introduced at the transceivers. Moreover, sufficient prefix and suffix length is not always guaranteed in order to improve the bandwidth efficiency of the system. In this section, we will first derive the system model by taking all aforementioned imperfections into consideration. The system performance is analysed in terms of power of desired signal, ICI, ISI and noise. Finally, new iterative equalization algorithms are proposed to mitigate the effect of interference and noise.

A. System Model in the Presence of Imperfection

In the presence of TO effect and insufficient guard time sequence, the derivation for DCT-MCM system in Section III using matrix operations are no longer suitable for imperfection analysis. Therefore, we will use discrete series in time domain to express the generalized model in this section. The discrete time sequence of a transmitted block is clearly shown in Eq. (2). Considering the introduced inter-block interference due to system imperfection, the corresponding discrete time series is extended from single block case to consecutive ones, by which the mth sample in the ith transmitted block is given by

$$x_i(m) = \sum_{n=0}^{N-1} a_{i,n}\beta_n \cos[\frac{\pi n(2m+1)}{2N}], \quad m = -v, \cdots, N \cdots, N+v-1. \tag{30}$$

For each transmitted block of $N+2v$ time-domain samples passing through the channel, the receiver chooses N consecutive useful data samples in the middle to be processed further and discards the other $2v$ guard interval samples from the front-end side equally. Assuming the frame synchronization error is presented as sampling time offset Δk, the indices of the remaining N samples corresponding to the jth received block are $\{k-\Delta k+j(N+2v)|k=0,\cdots,N-1\}$. In that case, the remaining samples $r(k)$ of the jth received block after channel convolution and guard symbols removing is written as

$$r(k) = \sum_{i=-\infty}^{+\infty}\sum_{m=-v}^{N+v-1} x_i(m)h(k-m-i(N+2v)) + n(k), \quad k = -\Delta k+j(N+2v), \cdots, -\Delta k+j(N+2v)+N-1. \tag{31}$$

It is noted that, without loss of generality, we integrate channel convolution process with the pre-filtering operations in Eq. (31) and take $h(k)$ as a general effective symmetric CIR after pre-filtering. As the correlation property for $h(k)$ has already been proved in Eq. (15), for simplicity, we denote the effective channel autocorrelation function as $R(k) = E[h_k \cdot h_k^*]$ and yield the general correlation function:

$$E[h_{k_1} \cdot h_{k_2}^*] = [\delta(k_1-k_2)+\delta(k_1+k_2)-\delta(k_1)\delta(k_2)]R(k_1) \tag{32}$$

Here, the unit sample sequence $\delta(k)$ achieves the unit value of 1 if $k=0$ but remains 0 for $k \neq 0$. In the practical design of a typical OFDM based system, a training sequence is usually employed in front of each symbol for the sake of estimating the parameters of imperfections. This kind of imperfection detection mechanism could be applied to DCT-MCM as well. In the following, the knowledge for CFO and TO is assumed to have been acquired from the training symbols.

B. Power of desired Signal, ICI, ISI and noise

In the following process, we focus on the data symbols detection within the intended received block ($j=0$). Due to fading effect caused by multipath, the output of DCT performed as demultiplexing is corrupted by interference plus the channel noise. Assuming the data symbols are statistically independent with unit average energy and the transmitted average energy per symbol equals to E_s. The power of desired signal received at the nth output of the DCT can be expressed in terms of desired signal, ISI, ICI, and coloured noise as follows:

$$P_x(n) = E_s\frac{N}{N+2v}(P_U(n)+P_{ICI}(n)+P_{ISI}(n))+V_n \tag{33}$$

The useful power P_U denotes the contribution from the desired symbol $a_{0,n}$. The ICI power P_{ICI} contains the contribution from the other symbols transmitted in the considered transmission block ($i=0$), whereas the ISI power P_{ISI} contains the contribution power from all subcarriers within other transmission blocks ($i \neq 0$). Finally, V_n denotes the contribution from the coloured noise defined in Eq. (26). Assuming the neighbouring subcarriers are modulated, we obtain

$$\begin{aligned} P_U(n) &= E[|\gamma(n,0,n)|^2] \\ P_{ICI}(n) &= \sum_{l=0,l\neq n}^{N-1} E[|\gamma(n,0,l)|^2] \\ P_{ISI}(n) &= \sum_{i=-\infty,i\neq 0}^{+\infty}\sum_{l=0}^{N-1} E[|\gamma(n,i,l)|^2] \end{aligned} \tag{34}$$

where $\gamma(n,i,l)$, given by

$$\gamma(n,i,l) = \beta_l\beta_n\sum_{k=0}^{N-1}\sum_{m=-v}^{N+v-1}\cos\frac{\pi(2m+1)(l+\Delta f)}{2N} \cdot \cos\frac{\pi(2k+1)n}{2N}h(k-\Delta k-m-i(N+2v)) \tag{35}$$

denotes the signal component for the demultiplexed output at nth subcarrier during the intended received block $j=0$, caused by the information symbol $a_{i,l}$ multiplexed on the lth subcarrier with carrier offset Δf considered during the ith transmission block. In order to distinguish the signal component from desired subcarrier and interference subcarriers separately, let us denote $\gamma(n,0,n)$ ($i=0, l=n$) as the desired signal power coefficient and the rest of $\gamma(n,i,l)$ are the interference power coefficients. For the calculation of the component $E[|\gamma(n,i,l)|^2]$, after substituting Eq. (32) into (35), we provide a computational efficient expression for $E[|\gamma(n,i,l)|^2]$ by dividing it into six sub-components (see Appendix B):

$$\begin{aligned} E|\gamma(n,i,l)|^2 = {} & E|\gamma_1(n,i,l)|^2 + E|\gamma_2(n,i,l)|^2 \\ & + E|\gamma_3(n,i,l)|^2 + E|\gamma_4(n,i,l)|^2 \\ & + E|\gamma_5(n,i,l)|^2 - E|\gamma_6(n,i,l)|^2 \end{aligned} \tag{36}$$

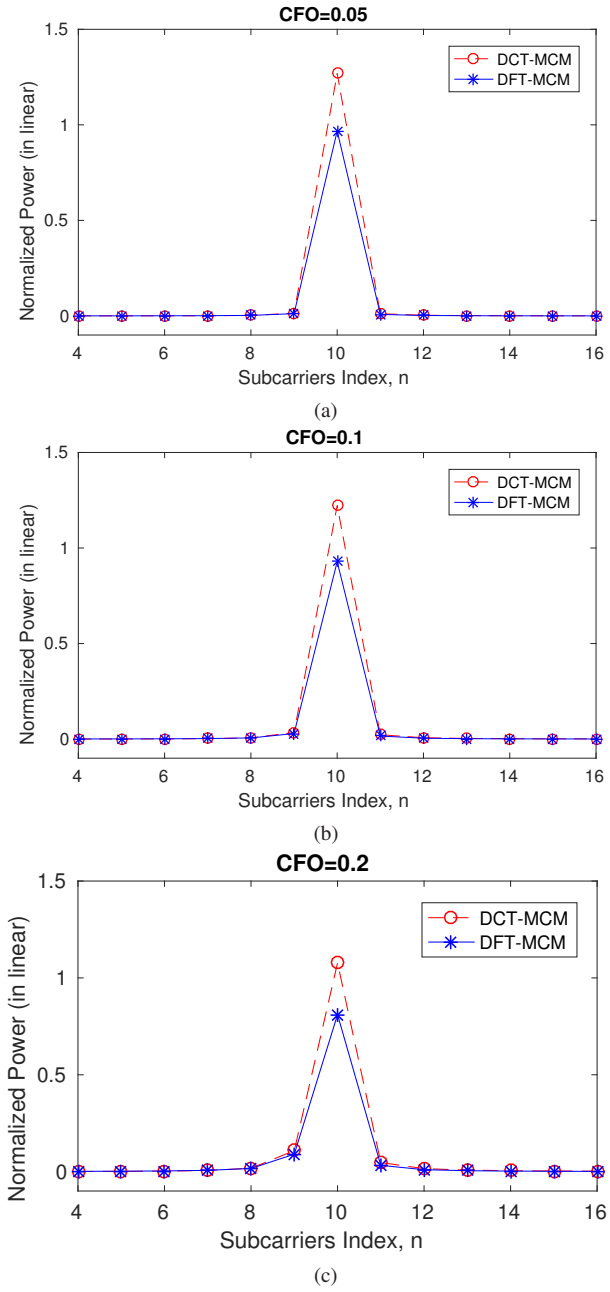

Fig. 5. Power spectrum (in linear) on the 10th subcarrier for DCT-MCM and DFT-MCM systems.(a)ΔfT=0.05. (b)ΔfT=0.1. (c)ΔfT=0.2.

In the presence of interference for the non-synchronized DCT-MCM system, the signal-to-interference ratio (SIR) of the nth subcarrier can be written as:

$$SIR(n) = \frac{P_u(n)}{P_{ICI}(n) + P_{ISI}(n)} \tag{37}$$

It is well known that DCT owns the advantage of energy compaction capabilities [12]. That is, the signal energy is mainly distributed in a few DCT coefficients, while the remaining coefficients are negligibly small. In this regard, [12] has shown that the DCT operation distributes more energy to the desired subcarrier and less energy to the ICI than the DFT operation under AWGN channel. This superiority can be also verified for multipath environments in Fig. 5 where the simulation channel complies with former IEEE 802.11 one. To highlight the the power spectrum distinction between DCT-MCM and DFT-MCM, we choose the 10th subcarrier as an example for the desired subcarrier in a 64-subcarrier system and show its power spectrum coefficients $E[|\gamma(n,0,10)|^2]$ from subcarrier index $n = 4$ to 16. The remaining coefficients are sufficiently small to be ignored, and are not plotted in the figure. In the presence of normalised frequency offset, ΔfT=0.05, 0.1 and 0.2 are presented for power spectrum comparison, respectively.

As can be seen in Fig. 5, for smaller absolute frequency offset, DCT-MCM shows better energy compaction property than DFT-MCM. Due to correlated filtering, the central desired subcarrier power can even be amplified to 1.4 times whereas DFT-MCM can only close to unit. However, by increasing the normalised frequency offset, the SIR for DCT-MCM will dramatically decrease and finally suffers higher ICI than that of DFT-MCM, which concurs with the results given in [12] under AWGN case.

In terms of the desire signal power P_U and ICI power P_{ICI}, Fig. 6 demonstrates the interference effect introduced by CFO and TO individually. In the case of CFO=0.05, P_U in DCT-MCM still see non-linear power distribution among subcarrier index due to filtering effect. This distributed desired signal power is higher in DCT-MCM while the interference noise P_{ICI} are almost under the same level for both two systems. On the other hand, Fig. 6(b) depicts the power variation property from TO perspective. As shown in the figure, the P_U curve has very similar distribution trend with cosine waves and the P_{ICI} is the other way around. Some sensitive subcarrier indexes (e.g n=18, 49) experience deep fading with maximum ICI noise. Nevertheless, in practical system design, since channel coding and interleaving techniques are involved, this kind of impairment can be remitted without much BER performance degradation.

C. Efficient Equalization Algorithm

With the provision of a complete signal model taking all the CFO, TO and insufficient guard sequence into consideration for DCT-MCM system under multipath environments, we can get the expression for the desired symbol on the nth subcarrier of the intended received block ($j = 0$)

$$\begin{aligned} y_{0,n} &= \gamma(n,0,n)a_{0,n} + \sum_{l=0,l\neq n}^{N-1} \gamma(n,0,l)a_{0,l} \\ &+ \sum_{i=-\infty,i\neq 0}^{+\infty} \sum_{l=0}^{N-1} \gamma(n,i,l)a_{i,l} + V_n \end{aligned} \tag{38}$$

As can be seen in Eq. (38), with certain level of imperfections introduced the received symbol $y_{0,n}$ will suffer from inner-block and inter-block interference plus coloured noise. The coloured noise has been analysed on the effect of pre-filtering and corresponding compensation methods have been proposed for optimum performance. But the interference will render the channel equalization matrix non-diagonal by which huge computational complexity has to be involved due to the inversion of channel equalization matrix especially when N

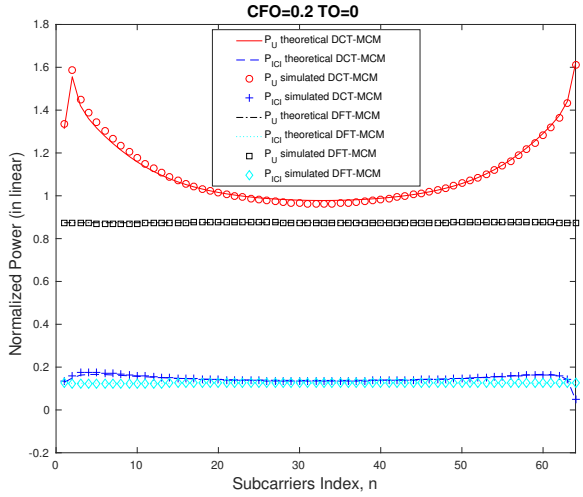

(a)

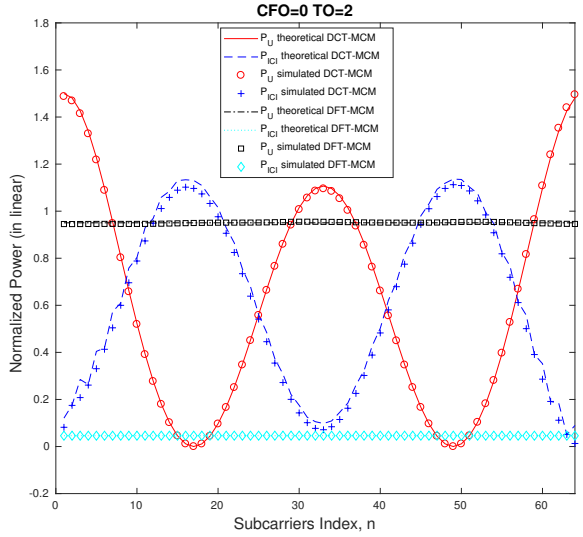

(b)

Fig. 6. Power of P_U and P_{ICI} in different subcarriers for DCT-MCM and DFT-MCM in the presence of transceiver imperfection. (a) CFO=0.2, TO=0. (b)CFO=0, TO=2.

is fairly large. On the other hand, the overall effective noise is no longer channel noise dominated, resulting ML method out of use in this case.

In the sequel, we first modify our channel equalization function for the ZF method. The other two performance enhanced methods MMSE and ML are then updated by the iteration results from a ZF equalizer. By regarding the correlated interference term as an additional part of the overall effective noise, we can avoid very complex joint-detection process. Consequently, the desired symbol $a_{0,n}$ that transmitted on the nth subcarrier in the intended received block $j = 0$ can be recovered through the modified ZF equalizer by the expression in terms of its desired signal component coefficient as

$$W_{0,n}^{ZF} = \gamma(n,0,n)^H / |\gamma(n,0,n)|^2 \tag{39}$$

However, for MMSE and ML equalizers, since the interference is correlated with desired subcarrier, direct equalizing operation incurs huge computational burden due to the destroyed orthogonal condition. And the channel equalizer matrix is no longer strictly diagonally dominant. To achieve optimum error rate performance as well as reduced equalization complexity, a ZF-based iterative technique is employed to address this problem.

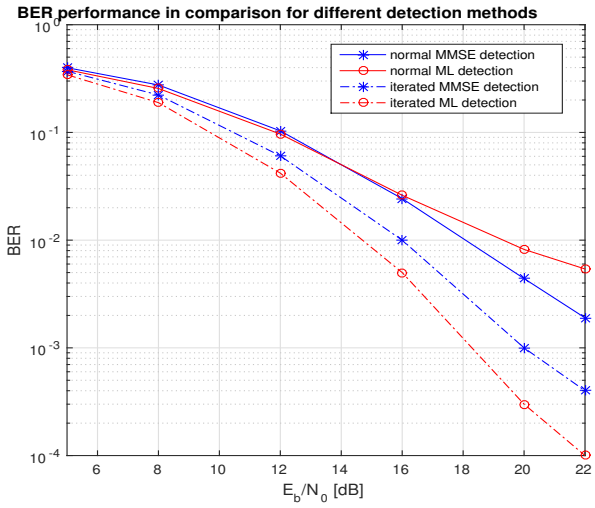

Fig. 7. BER performance for 8ASK DCT-MCM in normal and iterative detection methods in the presence of imperfections.

With the provision of a typical ZF equalizer function in Eq. (39), we yield the equalized symbol $\tilde{x}_{0,n} = y_{0,n} \cdot W_{0,n}^{ZF}$. Supposing the recovered symbol from $\tilde{x}_{0,n}$ after a de-mapper is $\tilde{a}_{0,n}$, we can estimate the interference term by feeding back the recovered symbols $\tilde{a}_{0,n}$ with their corresponding interference power coefficients

$$n_{0,n}^{IFC} = \sum_{l=0,l\neq n}^{N-1} \gamma(n,0,l)\tilde{a}_{0,l} + \sum_{i=-\infty,i\neq 0}^{+\infty} \sum_{l=0}^{N-1} \gamma(n,i,l)\tilde{a}_{i,l} \tag{40}$$

As aforementioned energy-compaction property of DCT, the desired signal power is highly concentrated on the modulated subcarrier and its few neighbouring subcarriers. This means most of the interference power coefficients are not significant and there is no need to calculate every interference term. Hence, we may relax the constraint to approximate the overall interference noise by making the following definition:

$$\tilde{\gamma}(n,i,l) = \begin{cases} = \gamma(n,i,l) & \text{if } \gamma(n,i,l) > \xi\gamma(n,0,n); \\ \approx 0 & \text{if } \gamma(n,i,l) \leq \xi\gamma(n,0,n). \end{cases} \tag{41}$$

where ξ is the interference power impact factor which allows flexibility for the balance between complexity and accuracy. Extensive tested results indicate a value of 3% for ξ is applicable for most cases where good approximation of interference noise can be obtained with very few terms. The approximate interference noise is thus formulated as

$$\tilde{n}_{0,n}^{IFC} = \sum_{l=0,l\neq n}^{N-1} \tilde{\gamma}(n,0,l)\tilde{a}_{0,l} + \sum_{i=-\infty,i\neq 0}^{+\infty} \sum_{l=0}^{N-1} \tilde{\gamma}(n,i,l)\tilde{a}_{i,l} \tag{42}$$

By eliminating the interference noise before equalizer, the sparse effective channel equalization matrix now becomes

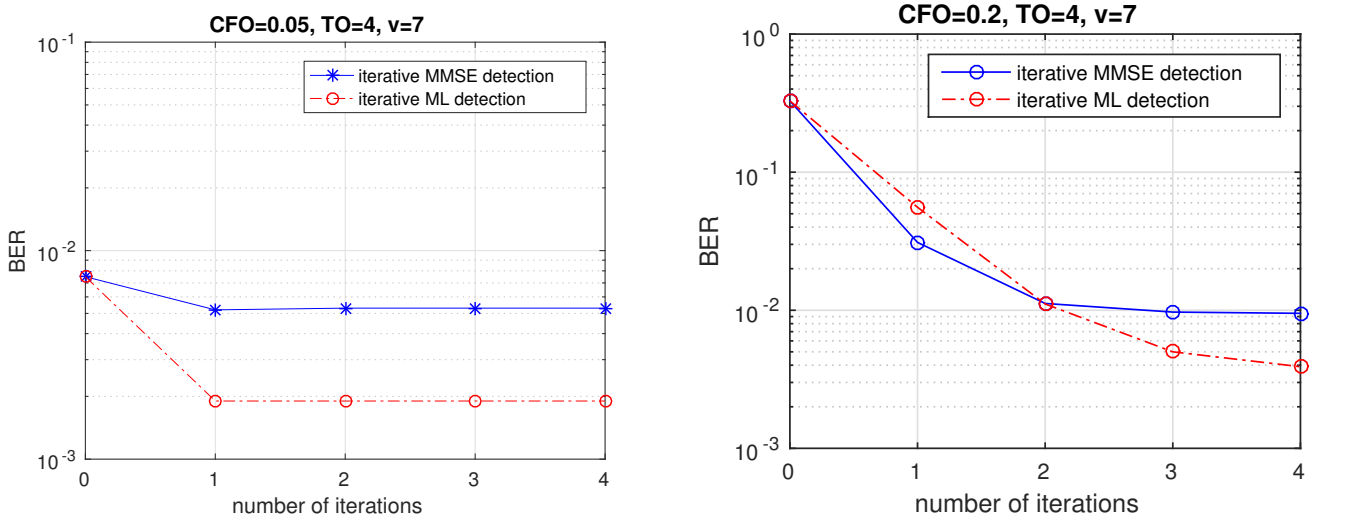

(a) (b)

Fig. 8. BER performance at E_b/N_o=16dB for MMSE and ML detections for 8ASK DCT-MCM in the presence of imperfections (a) CFO=0.05, TO=4, v=7. (b) CFO=0.2, TO=4, v=7.

diagonally dominant. Consequently, upon invoking the MMSE criterion in Eq. (27), the equalized symbol can be yield by

$$\tilde{x}_{0,n}^{MMSE} = (y_{0,n} - \tilde{n}_{0,n}^{IFC}) \frac{\sigma_s^2 \gamma(n,0,n)^H}{\sigma_s^2 |\gamma(n,0,n)|^2 + V_n} \tag{43}$$

For the ML method, equalization function in Eq. (29) is updated to:

$$\begin{aligned} L_i &= \ln \frac{\sum_{a_{0,n} \in \mathcal{A}_i^{(1)}} \exp(\frac{-|\tilde{y}_{0,n} - \gamma(n,0,n) a_{0,n}|^2}{V_n})}{\sum_{a_{0,n} \in \mathcal{A}_i^{(0)}} \exp(\frac{-|\tilde{y}_{0,n} - \gamma(n,0,n) a_{0,n}|^2}{V_n})} \\ &= \frac{V_n}{|\gamma(n,0,n)|^2} \{ - \min_{a_{0,n} \in \mathcal{A}_i^{(1)}} (\tilde{z}_{0,n} - a_{0,n})^2 \\ &\quad + \min_{a_{0,n} \in \mathcal{A}_i^{(0)}} (\tilde{z}_{0,n} - a_{0,n})^2 \} \end{aligned} \tag{44}$$

where $\tilde{y}_{0,n} = y_{0,n} - \tilde{n}_{0,n}^{IFC}$ and $\tilde{z}_{0,n} = \tilde{y}_{0,n}/\gamma(n,0,n)$. However, this equalization algorithm only works well when the interference is moderate. In the case of hardware impairment where ICI and ISI account for significant power loss, in order to estimate the interference accurately, it is benefit to update our new demodulated results and iterate them over Eq. (43) and (44) for several times.

The ZF-based iterative interference cancellation detections are verified by BER performance under comparison with normal detection methods. The simulation environment complies with what we assumed in Section III. In the presence of imperfections, we simulate the DCT-MCM system with CFO=0.2, TO=2 and reduce the prefix and suffix length from 12 to 7 (channel length is 11). As can be seen in Fig. 7, the new proposed iterative detection methods can successfully cancellate the ICI and ISI interference and therefore significantly improve the system performance by only one iteration. A 2 dB gain is achieved by the iterative MMSE equalizer while the iterative ML method shows even better attractive improvements, which demonstrates around 3 dB gain superiority than the iterative MMSE equalizer.

Fig. 8, on the other hand, shows the convergence property at E_b/N_o=16dB. Noted that the number of iterations at zero means the results are ZF based and has not yet iterated to MMSE and ML cases. As can be seen from the figure, if the interference level is moderate (e.g. CFO=0.05, TO=4, v=7) to the transmitted signal power, single iteration is sufficient to achieve the optimum performance, which is clearly identified in Fig. 8(a). However, when imperfection errors play dominant role (e.g. CFO=0.2, TO=4, v=7), increasing the number of iterations may be appropriately adjusted for striking a flexible trade off between the performance gain obtained and the complexity burden imposed, especially for ML method as verified in Fig. 8(b).

VI. Conclusion

In this paper, we first modelled the DCT-MCM systems with several constraint conditions satisfied to achieve interference free transmission. The boundaries for output SNR gain between two to three folds is verified for all subcarriers. As to the detectors, criterion for MMSE and ML methods are reformulated for DCT-MCM systems respectively. Simulation results illustrate the performance superiority of DCT-MCM than DFT-MCM systems when operating far from the capacity limit. In the presence of transceiver imperfections, we show that the advantage of energy compaction property by DCT still holds over multipath channels. In order to combat the interference arising from imperfection errors, new iterative equalization algorithms are proposed to effectively improve the performance of one-tap channel equalization algorithms. In the case of severe conditions where ICI and ISI are dominated, the proposed algorithms are able to mitigate the interference effect by adjusting the number of iteration times. An interesting topic for future research is to derive the exact theoretical BER performance for the prefiltering DCT-MCM systems.

REFERENCES

[1] R. V. Nee and R. Prasad, "OFDM for wireless multimedia communications", *Artech House, Boston, USA*, 2000.

[2] L. Zhang, P. Xiao, and A. Quddus, "Cyclic prefix based universal filtered multi-carrier system and performance analysis", *IEEE Signal Processing Letters*, vol. 23, no. 9, pp. 1197–1201, Sept 2016.

[3] L. Zhang, A. Ijaz, P. Xiao, A. Quddus, and R. Tafazolli, "Subband filtered multi-carrier systems for multi-service wireless communications", *IEEE Transactions on Wireless Communications*, vol. 16, no. 3, pp. 1893–1907, March 2017.

[4] L. Zhang, A. Ijaz, P. Xiao, and R. Tafazolli, "Multi-service system: An enabler of flexible 5G air interface", *IEEE Communications Magazine*, vol. 55, no. 10, pp. 152–159, October 2017.

[5] N. Michailow, M. Matth, I. S. Gaspar, A. N. Caldevilla, L. L. Mendes, A. Festag, and G. Fettweis, "Generalized frequency division multiplexing for 5th generation cellular networks", *IEEE Transactions on Communications*, vol. 62, no. 9, pp. 3045–3061, Sept 2014.

[6] B. Farhang-Boroujeny, "OFDM versus filter bank multicarrier", *IEEE Signal Processing Magazine*, vol. 28, no. 3, pp. 92–112, May 2011.

[7] L. Zhang, P. Xiao, A. Zafar, A. u. Quddus, and R. Tafazolli, "FBMC system: An insight into doubly dispersive channel impact", *IEEE Transactions on Vehicular Technology*, vol. 66, no. 5, pp. 3942–3956, May 2017.

[8] X. Zhang, M. Jia, L. Chen, J. Ma, and J. Qiu, "Filtered-OFDM- enabler for flexible waveform in the 5th generation cellular networks", pp. 1–6, Dec 2015.

[9] M. Rodrigues and I. Darwazeh, "Fast OFDM: A proposal for doubling the data rate of OFDM schemes", *IEEE/IEE International Conference on Telecommunications*, pp. 484–487, 2002.

[10] W.H Chen, C. Smith, and S. Fralick, "A fast computational algorithm for the discrete cosine transform", *IEEE Transactions on Communications*, vol. 25, no. 9, pp. 1004–1009, Sep 1977.

[11] Zhongde Wang, "Fast algorithms for the discrete W transform and for the discrete fourier transform", *IEEE Transactions on Acoustics, Speech, and Signal Processing*, vol. 32, no. 4, pp. 803–816, Aug 1984.

[12] P. Tan and N. C. Beaulieu, "A comparison of DCT-based OFDM and DFT-based OFDM in frequency offset and fading channels", *IEEE Transactions on Communications*, pp. 2113–2125, Nov 2006.

[13] W. A. Martins and P. S. R. Diniz, "DHT-based transceivers with reduced redundancy", *IEEE Transactions on Signal Processing*, vol. 60, no. 11, pp. 6080–6085, Nov 2012.

[14] R. Merched, "On OFDM and single-carrier frequency-domain systems based on trigonometric transforms", *IEEE Signal Processing Letters*, vol. 13, no. 8, pp. 473–476, Aug 2006.

[15] W.A. Martins and P.S.R. Diniz, "Memoryless block transceivers with minimum redundancy based on Hartley transforms", *Signal Processing*, pp. 240–251, 2011.

[16] H. Shariatmadari, R. Ratasuk, S. Iraji, A. Laya, T. Taleb, R. Jntti, and A. Ghosh, "Machine-type communications: current status and future perspectives toward 5G systems", *IEEE Communications Magazine*, vol. 53, no. 9, pp. 10–17, September 2015.

[17] Dian Fan, Z. Zhong, Gongpu Wang, and Feifei Gao, "Doppler shift estimation for high-speed railway wireless communication systems with large-scale linear antennas", pp. 96–100, Oct 2015.

[18] N. Al-Dhahir, H. Minn, and S. Satish, "Optimum DCT-based multicarrier transceivers for frequency-selective channels", *IEEE Transactions on Communications*, vol. 54, no. 4, pp. 760–760, April 2006.

[19] X. Ouyang and J. Zhao, "Single-tap equalization for fast OFDM signals under generic linear channels", *IEEE Communications Letters*, vol. 18, no. 8, pp. 1319–1322, Aug 2014.

[20] S. A. Martucci, "Symmetric convolution and the discrete sine and cosine transforms", *IEEE Transactions on Signal Processing*, vol. 42, no. 5, pp. 1038–1051, May 1994.

[21] J. Zhao and A. Ellis, "Transmission of 4-ASK optical fast OFDM with chromatic dispersion compensation", *IEEE Photonics Technology Letters*, vol. 24, no. 1, pp. 34–36, Jan 2012.

[22] G. D. Mandyam, "Sinusoidal transforms in OFDM systems", *IEEE Transactions on Broadcasting*, vol. 50, no. 2, pp. 172–184, June 2004.

[23] F. CruzRoldan, M. E. Dominguez Jimenez, G. Sansigre Vidal, D. Luengo, and M. Moonen, "DCT-based channel estimation for single and multicarrier communications", *Signal Processing*, vol. pp, no. 128, pp. 332–339, Nov 2016.

[24] Chang He, L. Zhang, J. Mao, Aijun Cao, P. Xiao, and M. A. Imran, "Output SNR analysis and detection criteria for optimum DCT-based multicarrier system", *2016 International Symposium on Wireless Communication Systems (ISWCS)*, pp. 59–64, Sept 2016.

[25] V. Sanchez, P. Garcia, A. M. Peinado, J. C. Segura, and A. J. Rubio, "Diagonalizing properties of the discrete cosine transforms", *IEEE Transactions on Signal Processing*, pp. 2631–2641, Nov 1995.

[26] F. Cruz-Roldan, M. E. Dominguez-Jimenez, G. Sansigre Vidal, P. Amo-Lopez, M. Blanco-Velasco, and . Bravo-Santos, "On the use of discrete cosine transforms for multicarrier communications", *IEEE Transactions on Signal Processing*, vol. 60, no. 11, pp. 6085–6090, Nov 2012.

[27] H. Steendam and M. Moeneclaey, "Analysis and optimization of the performance of OFDM on frequency-selective time-selective fading channels", *IEEE Transactions on Communications*, vol. 47, no. 12, pp. 1811–1819, Dec 1999.

[28] "IEEE standard for information technology- telecommunications and information exchange between systems-local and metropolitan area networks-specific requirements-part 11: Wireless LAN MAC and PHY specifications", *IEEE Std 802.11-1997*, pp. i–445, 1997.

[29] M. K. Ozdemir and H. Arslan, "Channel estimation for wireless OFDM systems", *IEEE Commun. Surveys Tuts.*, vol. 9, no. 2, pp. 18–48, 2007.

[30] A. Trimeche, N. Boukid, A. Sakly, and A. Mtibaa, "Performance analysis of ZF and MMSE equalizers for mimo systems", *7th International Conference in Design Technology of Integrated Systems*, pp. 1–6, May 2012.

[31] C. Y. Hung and W. H. Chung, "An improved MMSE-based MIMO detection using low-complexity constellation search", *2010 IEEE Globecom Workshops*, pp. 746–750, Dec 2010.

[32] J Mao, M. Abdullahi, and P. Xiao, "A low complexity 256QAM soft demapper for 5G mobile system", *EuCNC*, 2016.

APPENDIX A

Considering the effective channel coefficients are in symmetric after pre-filtering: $h_k = h_{-k}$, we firstly consider $E[h_i \cdot h_j]$ for the coefficients on the right side where $i \geq 0, j \geq 0$. The results then can be easily extended to the whole case.

1) when $i \neq j$, it is easy to verify $E[h_i]$ and $E[h_j]$ are uncorrelated to each other. Consequently, we yield: $E[h_i \cdot h_j] = 0$.
2) when $i = j \neq 0$, we have: $E[f_i^2 \cdot f_j^2] = E[f_i^2] \cdot E[f_j^2] = 0.25\sigma_i^2 \cdot \sigma_j^2$. In that case, $E[h_i \cdot h_j] = \sum_{p=0}^{i} E[f_p^2 \cdot f_{L-i+p}^2] = \sum_{p=0}^{i} E[f_p^2] \cdot E[f_{L-i+p}^2] = \frac{1}{4}\sum_{p=0}^{|i|} \sigma_p^2 \sigma_{L-|i|+p}^2$.
3) when $i = j = 0$, the expected value on fourth order for Gaussian variable is calculated by: $E[f_i^4] = 3 \cdot (\sqrt{0.5}\sigma_i)^4 = \frac{3}{4}\sigma_i^4$. Without loss of generality, $E[h_i \cdot h_j]$ then can be given by: $E[h_i \cdot h_j] = \sum_{p=0}^{L-1} E[f_p^4] + 2\sum_{t=0}^{L-1-p} E[f_p^2 \cdot f_{p+t}^2] = \frac{3}{4}\sum_{p=0}^{L-1} \sigma_p^4 + \frac{1}{2}\sum_{p=0}^{L-1}\sum_{t=0}^{L-1-p} \sigma_p^2 \sigma_{p+t}^2$.

By combining the above three conditions and extending them to the whole effective channel coefficients case, we obtain the following:

$$E[h_i \cdot h_j] = \begin{cases} \frac{1}{4}\sum_{p=0}^{|i|} \sigma_p^2 \sigma_{L-|i|+p}^2 & i = \pm j \neq 0; \\ \frac{3}{4}\sum_{p=0}^{L-1} \sigma_p^4 + \frac{1}{2}\sum_{p=0}^{L-1}\sum_{t=0}^{L-1-p} \sigma_p^2 \sigma_{p+t}^2 & i = j = 0; \\ 0 & \text{others.} \end{cases} \tag{45}$$

APPENDIX B

The output signal power on the in-phase branch at kth subcarrier is represented as:

$$E[H_k^2] = E[h_0^2] + 4\sum_{n=1}^{L-1} E[h_n^2] \cdot \cos^2[\frac{\pi}{N}nk] \tag{46}$$

which equals to

$$E[H_k^2] = E[h_0^2] + 2\sum_{n=1}^{L-1} E[h_n^2] \cdot (\cos[\frac{2\pi}{N}nk] + 1) \tag{47}$$

The function above now can be considered as a convex function optimization problem and it is easy to find $E[H_k^2]$ will achieve the lower peak value at the points $k/N = 1/4$ by taking its differentiation function $\frac{\partial \mathrm{E}[\mathrm{H}_\mathrm{k}^2]}{\partial \mathrm{k}} = 0$. As a consequence, the minimal value of $E[H_k^2]$ is

$$min\{E[H_k^2]\} = \frac{3}{4}\sum_{p=0}^{L-1} \sigma_p^4 + \frac{1}{2}\sum_{p=0}^{L-1}\sum_{t=0}^{L-1-p} \sigma_p^2 \sigma_{p+t}^2 (2 + (-i)^{2p} \cdot \frac{1-(-1)^p}{2}) \tag{48}$$

Considering σ_p^2 subject to the exponential power delay distribution in the Rayleigh fading channel, we have

$$min\{E[H_k^2]\} \geq \frac{3}{4}\sum_{p=0}^{L-1} \sigma_p^4 + \sum_{p=0}^{L-1}\sum_{t=0}^{L-1-p} \sigma_p^2 \sigma_{p+t}^2 = \frac{1}{4}\sum_{p=0}^{L-1} \sigma_p^4 + 0.5 \tag{49}$$

Recalling the Cauchy-Schwarz inequality theorem: $\sum_{i=1}^{n} a_i^2 \geq \frac{1}{n}(\sum_{i=1}^{n} a_i)^2$, we obtain the following

$$\frac{1}{4}\sum_{p=0}^{L-1} \sigma_p^4 \geq \frac{1}{4} \cdot \frac{1}{L}(\sum_{p=0}^{L-1} \sigma_p^2)^2 = \frac{1}{4L} \tag{50}$$

Combining the above results, we have $min\{E[H_k^2]\} \geq 0.5 + \frac{1}{4L}$. Accounting the other half of distributed signal power on quadrature branch, the lower bound of the minimal signal power gain is $1 + \frac{1}{2L}$.

APPENDIX C

Let us consider the calculation of the component $E|\gamma(n,i,l)|^2$. Without loss of generality, the general form for $E|\gamma(n,i,l)|^2$ is expressed as:

$$E|\gamma(n,i,l)|^2 = \beta_l^2\beta_n^2 \sum_{k,k'=0}^{N-1}\sum_{m,m'=-v}^{N+v-1} \cdot\frac{1}{4}[\cos\frac{\pi(l+\Delta f)(m+m'+1)}{N} + \cos\frac{\pi(l+\Delta f)(m-m')}{N}] \cdot [\cos\frac{\pi n(k+k'+1)}{N}$$
$$+\cos\frac{\pi n(k-k')}{N}] \cdot [\delta(k-k'-m+m') + \delta(k+k'-m-m'-2\Delta k) - \delta(k-m-\Delta k)\cdot\delta(k'-m'-\Delta k)]R(k-m-\Delta k) \quad (51)$$

For simplicity, we make new summation variables: $m+m'=u_1$, $m-m'=u_2$, $k+k'=u_3$ and $k-k'=u_4$. By defining the inner weight function: $A_{l,n}(u_1,u_2,u_3,u_4) = \frac{1}{4}[\cos\frac{\pi(l+\Delta f)(u_1+1)}{N} + \cos\frac{\pi(l+\Delta f)u_2}{N}] \cdot [\cos\frac{\pi n(u_3+1)}{N} + \cos\frac{\pi n u_4}{N}]$, we obtain:

$$\begin{aligned}
E|\gamma(n,i,l)|^2 &= \beta_l^2\beta_n^2 \sum_{u_1}\sum_{u_2}\sum_{u_3}\sum_{u_4} A_{l,n}(u_1,u_2,u_3,u_4)\cdot[\delta(u_4-u_2)+\delta(u_3-u_1-2\Delta k)-\delta(k-m-\Delta k)\\
&\quad \cdot\delta(k'-m'-\Delta k)]R(k-m-\Delta k)\\
&= \beta_l^2\beta_n^2[\sum_{u_1}\sum_{u_2}\sum_{u_3} A_{l,n}(u_1,u_2,u_3,u_2) + \sum_{u_2}\sum_{u_3}\sum_{u_4} A_{l,n}(u_3-2\Delta k,u_2,u_3,u_4)\\
&\quad -\sum_{u_2}\sum_{u_3} A_{l,n}(u_3-2\Delta k,u_2,u_3,u_2)]\cdot R(k-m-\Delta k)\\
&= \beta_l^2\beta_n^2[\sum_{u_2=0}^{N-1}\sum_{u_1}\sum_{u_3} A_{l,n}(u_1,u_2,u_3,u_2) + \sum_{u_2=-(N-1)}^{-1}\sum_{u_1}\sum_{u_3} A_{l,n}(u_1,u_2,u_3,u_2)\\
&\quad +\sum_{u_3=0}^{N-1}\sum_{u_2}\sum_{u_4} A_{l,n}(u_3-2\Delta k,u_2,u_3,u_4) + \sum_{u_3=N}^{N+2\Delta k-1}\sum_{u_2}\sum_{u_4} A_{l,n}(u_3-2\Delta k,u_2,u_3,u_4)\\
&\quad +\sum_{u_3=N+2\Delta k}^{2N-2}\sum_{u_2}\sum_{u_4} A_{l,n}(u_3-2\Delta k,u_2,u_3,u_4)\\
&\quad -\sum_{u_2}\sum_{u_3} A_{l,n}(u_3-2\Delta k,u_2,u_3,u_2)]\cdot R(k-m-\Delta k)\\
&= E|\gamma_1(n,i,l)|^2 + E|\gamma_2(n,i,l)|^2 + E|\gamma_3(n,i,l)|^2 + E|\gamma_4(n,i,l)|^2\\
&\quad +E|\gamma_5(n,i,l)|^2 - E|\gamma_6(n,i,l)|^2
\end{aligned} \quad (52)$$

whereas the six components of $E|\gamma(n,i,l)|^2$ are given by:

$$\begin{aligned}
E|\gamma_1(n,i,l)|^2 &= \beta_l^2\beta_n^2 \sum_{u_2=0}^{N-1}\sum_{u_1}\sum_{u_3} A_{l,n}(u_1,u_2,u_3,u_2)\cdot R(k-m-\Delta k)\\
&= \beta_l^2\beta_n^2 \sum_{u_2=0}^{N-1}\sum_{u_1=-v}^{N+v-u_2-1}\sum_{u_3=u_2}^{N-1} A_{l,n}(2u_1+u_2,u_2,-u_2,u_2)\cdot R(u_3-u_2-u_1-\Delta k)
\end{aligned} \quad (53)$$

$$\begin{aligned}
E|\gamma_2(n,i,l)|^2 &= \beta_l^2\beta_n^2 \sum_{u_2=-(N-1)}^{-1}\sum_{u_1}\sum_{u_3} A_{l,n}(u_1,u_2,u_3,u_2)\cdot R(k-m-\Delta k)\\
&= \beta_l^2\beta_n^2 \sum_{u_2=-N+1}^{-1}\sum_{u_1=-v}^{N+v+u_2-1}\sum_{u_3=-u_2}^{N-1} A_{l,n}(2u_1-u_2,u_2,2u_3+u_2,u_2)\cdot R(u_3+u_2-u_1-\Delta k)
\end{aligned} \quad (54)$$

$$\begin{aligned}
E|\gamma_3(n,i,l)|^2 &= \beta_l^2\beta_n^2 \sum_{u_3=0}^{N-1}\sum_{u_2}\sum_{u_4} A_{l,n}(u_3-2\Delta k,u_2,u_3,u_4)\cdot R(k-m-\Delta k)\\
&= \beta_l^2\beta_n^2 \sum_{u_3=0}^{N-1}\sum_{u_4=0}^{u_3}\sum_{u_2=0}^{2v+u_3-2\Delta k} A_{l,n}(u_3-2\Delta k,2u_2-u_3-2v+2\Delta k,u_3,2u_4-u_3)\\
&\quad \cdot R(u_4-u_2+v-\Delta k)
\end{aligned} \quad (55)$$

$$
\begin{aligned}
E|\gamma_4(n,i,l)|^2 &= \beta_l^2\beta_n^2 \sum_{u_3=N}^{N+2\Delta k-1} \sum_{u_2}\sum_{u_4} A_{l,n}(u_3-2\Delta k,u_2,u_3,u_4)\cdot R(k-m-\Delta k) \\
&= \beta_l^2\beta_n^2 \sum_{u_3=N}^{N+2\Delta k-1} \sum_{u_4=0}^{2N-u_3-2} \sum_{u_2=0}^{2v+u_3-2\Delta k} A_{l,n}(u_3-2\Delta k, 2u_2-u_3-2v+2\Delta k, u_3, 2u_4-2N+2 \\
&\quad +u_3)\cdot R(u_4+u_3-u_2-N+v+1-\Delta k) \qquad (56) \\
E|\gamma_5(n,i,l)|^2 &= \beta_l^2\beta_n^2 \sum_{u_3=N+2\Delta k}^{2N-2} \sum_{u_2}\sum_{u_4} A_{l,n}(u_3-2\Delta k,u_2,u_3,u_4)\cdot R(k-m-\Delta k) \\
&= \beta_l^2\beta_n^2 \sum_{u_3=N+2\Delta k}^{2N-2} \sum_{u_4=0}^{2N-u_3-2} \sum_{u_2=0}^{2N+2v-u_3-2+2\Delta k} A_{l,n}(u_3-2\Delta k, 2u_2-2N-2v+2+u_3-2\Delta k, u_3, \\
&\quad 2u_4-2N+2+u_3)\cdot R(u_4-u_2+v+\Delta k) \qquad (57) \\
E|\gamma_6(n,i,l)|^2 &= \beta_l^2\beta_n^2 \sum_{u_2}\sum_{u_3} A_{l,n}(u_3-2\Delta k,u_2,u_3,u_2)\cdot R(k-m-\Delta k) \\
&= \beta_l^2\beta_n^2 \sum_{u_1=0}^{N-1}\sum_{u_2=0}^{N-1} \frac{1}{4}[\cos\frac{\pi(l+\Delta f)(u_1+u_2-2\Delta k+1)}{N} + \cos\frac{\pi(l+\Delta f)(u_1-u_2)}{N}] \\
&\quad [\cos\frac{\pi n(u_1+u_2+1)}{N} + \cos\frac{\pi n(u_1-u_2)}{N}]\cdot R(0) \qquad (58)
\end{aligned}
$$